Available online at www.sciencedirect.com
ScienceDirect
Trans. Nonferrous Met. Soc. China 24(2014) 303−309
Transactions of Nonferrous Metals Society of China
www.tnmsc.cn

Fatigue crack initiation and early propagation behavior of 2A97 Al−Li alloy

Jing ZHONG[1], Shen ZHONG[1], Zi-qiao ZHENG[1,2], Hai-feng ZHANG[1], Xian-fu LUO[1]

1. School of Materials Science and Engineering, Central South University, Changsha 410083, China;
2. Key Laboratory of Nonferrous Material Science and Engineering, Ministry of Education, Central South University, Changsha 410083, China

Received 23 February 2013; accepted 23 May 2013

Abstract: The fatigue crack initiation and early propagation behavior of 2A97 Al−Li alloy was studied. The smooth specimens were fatigued at room temperature under constant maximum stress control when stress ratio (R) is 0.1 and frequency (f) is 40 Hz. Microstructure observations were examined by optical microscopy, transmission electron microscopy, scanning electron microscopy and electron back scattered diffusion, in order to investigate the relationship between microstructure and fatigue crack initiation and early propagation behavior of 2A97 alloy. The results show that the fatigue cracks are predominantly initiated at inclusions and coarsen secondary phases on the surface of 2A97 alloy. The fatigue crack early propagation behavior of 2A97 alloy is predominantly influenced by the interactions between grain structure and dislocations or persistent slip bands (PSBs). When the misorientation of two neighbouring grains is close to the orientations of the favorable slip plane within these two grains, high-angle grain boundary severely hinders the PSBs passing through, and thus leads to crack bifurcation and deflection.

Key words: 2A97 Al−Li alloy; fatigue crack initiation; fatigue crack; early propagation

1 Introduction

The fatigue crack initiation behavior mainly depends on the irregular nature of fatigue cracks and the influence of metallurgical features such as inclusions and grain boundaries. Micromechanisms of fatigue crack initiation at inclusions depend on the matrix, types of inclusions and properties of the inclusion-matrix interface [1,2]. TANAKA and MURA [3] concluded three modes of fatigue crack initiation at inclusions in high strength alloys, which are dependent on the slip characteristics of the matrix, the distribution of inclusion size and the strength of the matrix-inclusion interface [4]. MORRIS and JAMES [5] observed that the inclusions were debonded firstly at the inclusion−matrix interface in 2219−T851 alloys under maximum cyclic stresses. The fatigue crack in 2024−T4 alloys could be initiated along slip bands emanating from an inclusion, which could not be debonded [6].

It is well known that grain boundary characteristic is one of the main barriers to the fatigue crack growth behaviour in most metallic structures, which especially often accounts for the short fatigue crack growth rate [7]. The short crack propagation behavior of Al−Li 8090 alloys [8,9] was dominated by the twist and tilt components of crack plane deflection at grain boundaries, which also explained the phenomena of fatigue branching. LIAO [10] presented a dislocation theory based short crack model to analyse the short crack growth behavior of Al 2024−T351 alloys by taking into account the influences of grain size, orientation and grain boundary.

The Al−Li alloys have been widely used in various structural components in the aircraft for their high specific strength and superior comprehensive performances [11,12]. The 2A97 alloy belongs to the third generation of Al−Li alloys, which has excellent corrosion resistance, superior damage tolerance and good weldability [13]. There is a broad prospect of application in the aerospace field, such as lower wing panel, fuselage and stringers. In the last ten years, several investigations have been carried out on the mechanical and corrosion behavior of 2A97 alloy [14−16], however, its fatigue behavior has not been investigated extensively. In this study, the mechanical and fatigue properties of 2A97 alloy were evaluated, including characterization of the fatigue crack initiation and micro-crack propagation

Corresponding author: Zi-qiao ZHENG; Tel: +86-731-88830270; Fax: +86-731-8876692; E-mail: s-maloy@mail.csu.edu.cn
DOI: 10.1016/S1003-6326(14)63061-2

behavior, based on the observation of microstructures by transmission electron microscopy (TEM), scanning electron microscopy (SEM) and electron back scattered diffusion (EBSD).

2 Experimental

The as-received materials are 40 mm thick rolled 2A97 alloy plate in T851 conditions with the base composition of 2.8% Cu, 0.35% Mg, 0.4% Mn, 0.5% Zn, 1.8% Li and 0.1% Zr (mass fraction). The tensile properties in LT direction are listed in Table 1. The grain structure was characterized using a combination of optical microscopy (OM) and orientation imaging microscopy (OIM).

Table 1 Tensile properties of 2A97−T851 alloy

σ_b/MPa	$\sigma_{0.2}$/MPa	δ/%	E/GPa
555	469	13	76

The thin foils for TEM observation were prepared with a standard procedure: samples were polished mechanically to less than 100 μm, and twin-jet was electro-polished using a 1/4 nitric acid and 3/4 methanol solution held at −25 to −35 °C, with a voltage of 25 V. The microstructures were observed on transmission electron microscopy (TEM, Tecnai G220) at an operating voltage of 200 kV.

The fatigue crack initiation tests were performed on MTS 858 servo-hydraulic fatigue testing machine at room temperature with the stress ratio (R) of 0.1 and frequency (f) of 40 Hz. All fatigue smooth specimens were taken from L−T direction of the as-received plate, and the specimen surfaces were precisely ground to avoid the influences of surface defects. The crack initiation samples were observed by scanning electron microscope (SEM, Quanta-200) equipped with an energy dispersive spectrometer (EDS). For EBSD measurement, the sample surface was polished electrolytically to eliminate the residual stress. EBSD examinations were carried out by scanning electron microscopy (SEM, H-3400) with TSL EBSD patterns detection system.

3 Results

3.1 Microstructures of 2A97 alloy

A typical pancake-shaped grain structure of 2A97 alloy showing partially recrystallization is displayed in Fig. 1, with large variation in grain width and grain aspect ratio in the three orthogonal directions. The grains are significantly flattened and elongated in rolling direction, and the grain dimensions in transverse direction are comparably smaller than those in longitudinal direction.

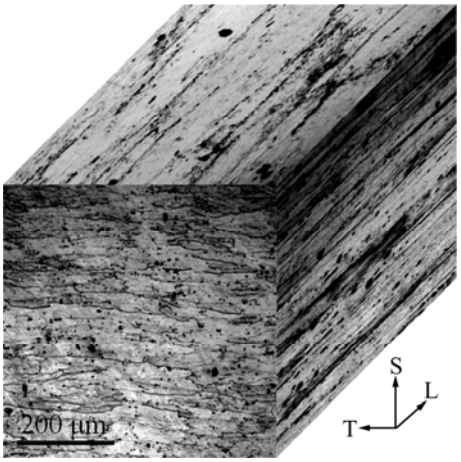

Fig. 1 Triplanar optical micrograph of 2A97−T851 alloy

The results of TEM observation of the predominant precipitates in 2A97 alloy are shown in Fig. 2. The dark center field image with ⟨001⟩ beam direction is shown in Fig. 2(a), which depicts a massive and uniform distribution of needle θ'' phases, spherical δ' phases. A few δ'/β' composite particles are also observed, with the typical dark core of β' enveloped by a bright shell of δ', forming the characteristic bull's eye structure [17,18]. Many fine dispersed $T1$ phases and a few S' phases can be seen in Fig. 2(b), which are observed from ⟨112⟩ beam direction. The morphologies in the vicinity of grain boundaries are shown in Figs. 2(c) and (d). An evidence of precipitation free zone of about 40 nm width can be seen, and the continuous equilibrium phases can also be observed along the high angle grain boundaries.

3.2 Fatigue crack initiation and early propagation

Figure 3 shows some typical sites for fatigue crack initiation in 2A97 fatigue smooth specimens obtained by SEM and the corresponding EDS results. Figure 3(a) shows a network of cracks initiated at metallic inclusions and propagated into the matrix after 8000 cycles with a maximum stress of 400 MPa. The EDS results in Fig. 3(b) indicate that they are chiefly constituted by the brittle aluminum oxides, which may generate in the smelting process. As shown in Fig. 3(c), a crack initiates at the interior of intermetallic particles, which might be $Al_7Cu_2(Fe,Mn)$ particles according to the EDS results in Fig. 3(d).

Figure 4 shows the typical SEM images of the fatigue crack initiation and early growth behavior on the specimen surface with the orientation of L−T. A cyclic loading with the maximum stress of 400 MPa and stress ratio of 0.1 is vibrated about 21000 cycles. It can be seen that the fatigue crack initiates at the specimen edge, where no evident large secondary phase is observed. Under the control of cycle stress, there is a large stress concentration near the sharp edge of the specimen,

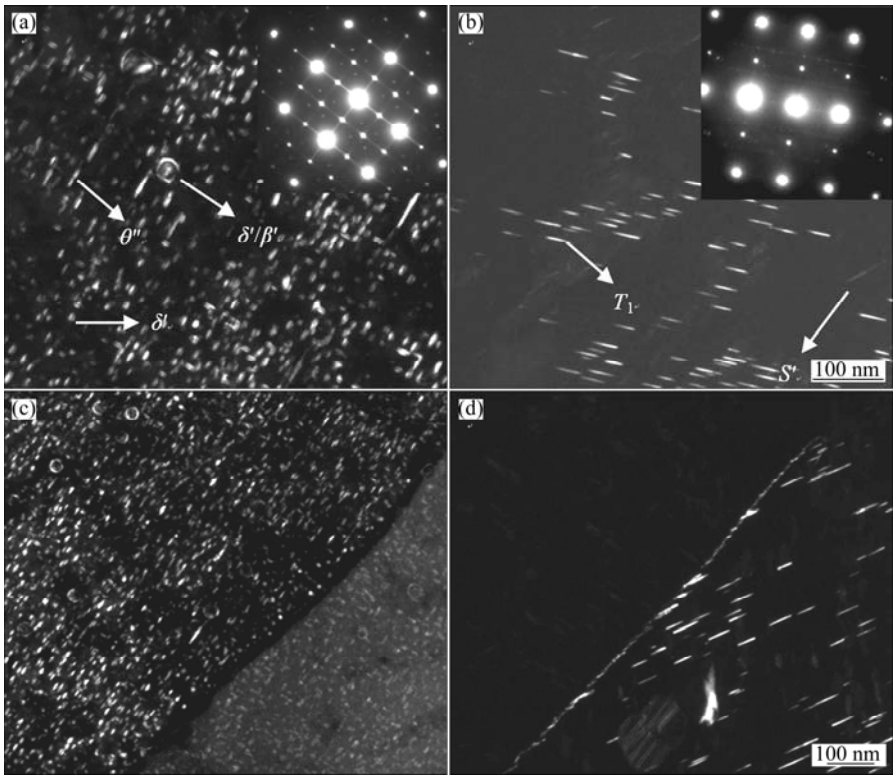

Fig. 2 TEM images showing typical precipitates of 2A97 alloy in dark field: (a) θ'' and δ' phase with corresponding SAED pattern from $\langle 001\rangle_\alpha$; (b) T_1 phase with corresponding SAED pattern from $\langle 112\rangle_\alpha$; (c) Precipitate-free zone (PFZ) and grain boundary precipitates from $\langle 001\rangle_\alpha$; (d) Precipitate-free zone (PFZ) and grain boundary precipitates from $\langle 112\rangle_\alpha$

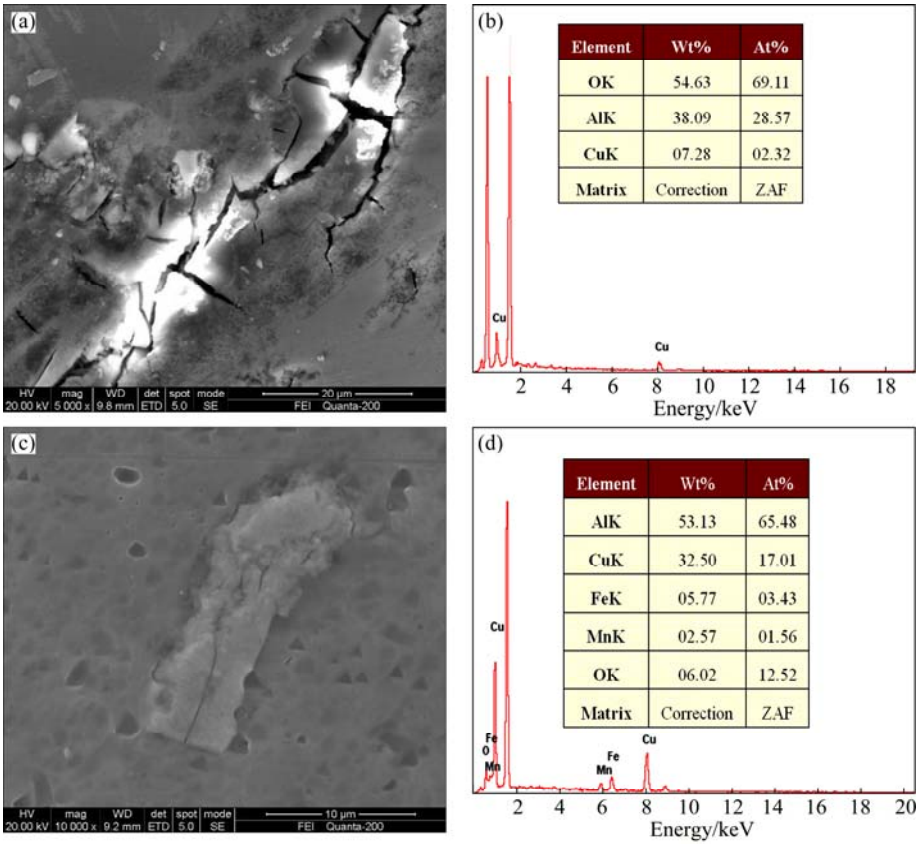

Fig. 3 SEM images for fatigue crack initiation: (a) A network of cracks initiated at inclusion of aluminum oxide; (b) Corresponding EDS results of (a); (c) A crack initiated in the secondary phase; (d) Corresponding EDS results of (c)

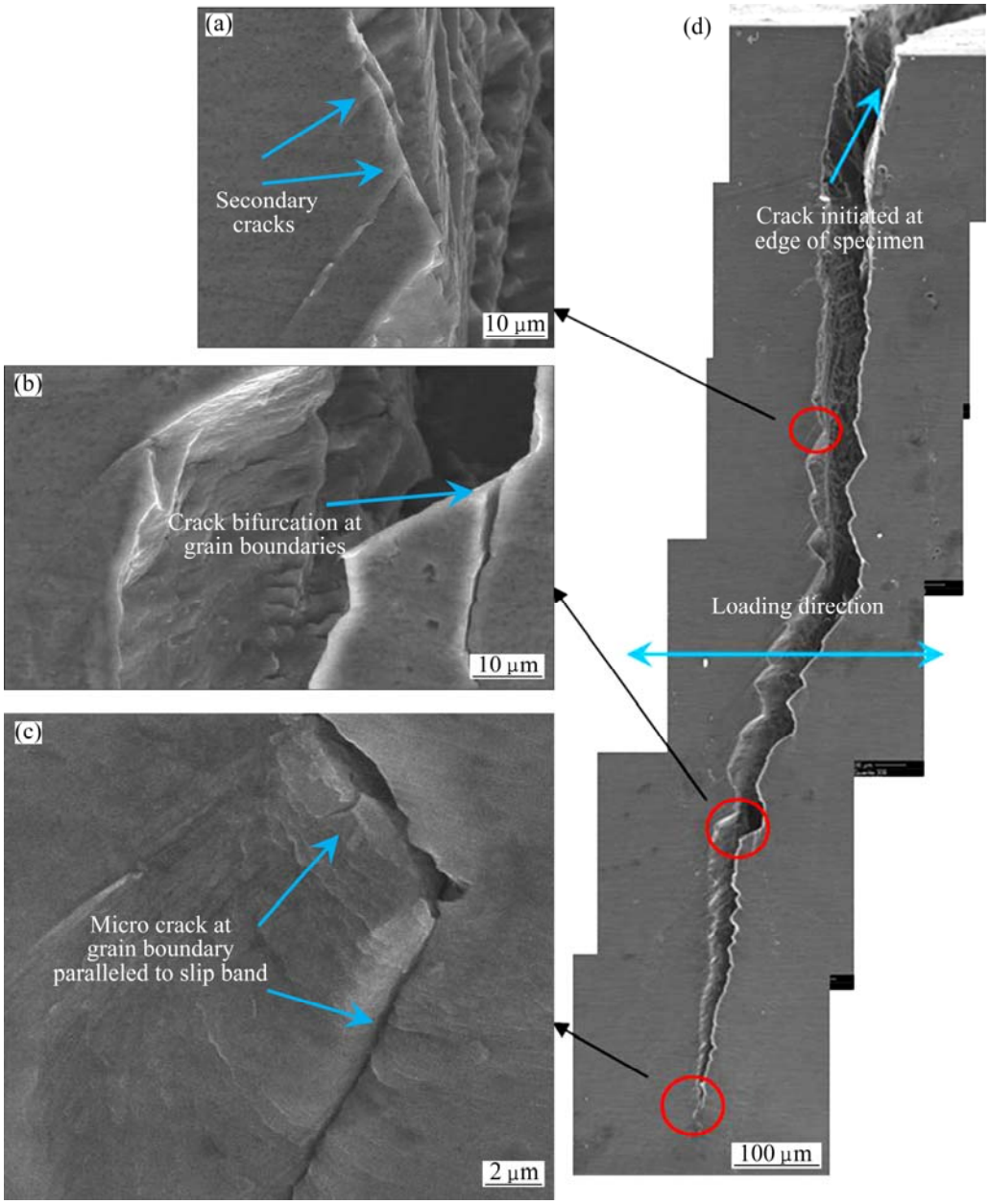

Fig. 4 SEM images of fatigue crack early growth behavior of 2A97 alloy with specimen orientation of L−T, about 21000 vibratory cycles, maximum stress of 400 MPa and stress ratio of 0.1: (a) Secondary cracks; (b) Crack bifurcation at grain boundary; (c) Micro crack initiated at grain boundary and parallel to slip bands; (d) Overall image

which would cause localized plastic deformation and lead to crack initiation. Typical images for secondary cracks and crack bifurcation can be observed in Figs. 4(a) and (b). Secondary cracks derived from the main crack, which might be brittle grain (or sub-grain) boundaries cracking under the influence of the strain field of crack tip. At the very tip of this crack, the occurrences of slip bands at a certain angle with the grain boundary can be seen obviously, as well as some micro-cracks parallel to them (Fig. 4(c)).

The EBSD results for the fatigue crack propagation paths of 2A97 alloy are shown in Fig. 5. The SEM image (Fig. 5(a)) for fatigue crack and grain/sub-grain boundaries shows that the crack moves through several different sized grains. There is a significant recrystallization in the region I, which is normally high-angle boundary grain. However, the recrystallization is not observed in the region II, which contains several low-angle boundary sub-grains. The fatigue crack moves through the region II without obvious deflection, while a tortuous deflection of fatigue crack can be seen when it moves through the region I. The grain orientation distribution in Fig. 5(b) shows that the prior path of crack expansion is along the sub-grain boundaries or grain boundaries, and larger deflections occur when the crack moves through a large angle grain boundaries (circle marked in Fig. 5(b)). The Schmid factor distribution in Fig. 5(c) represents that the crack

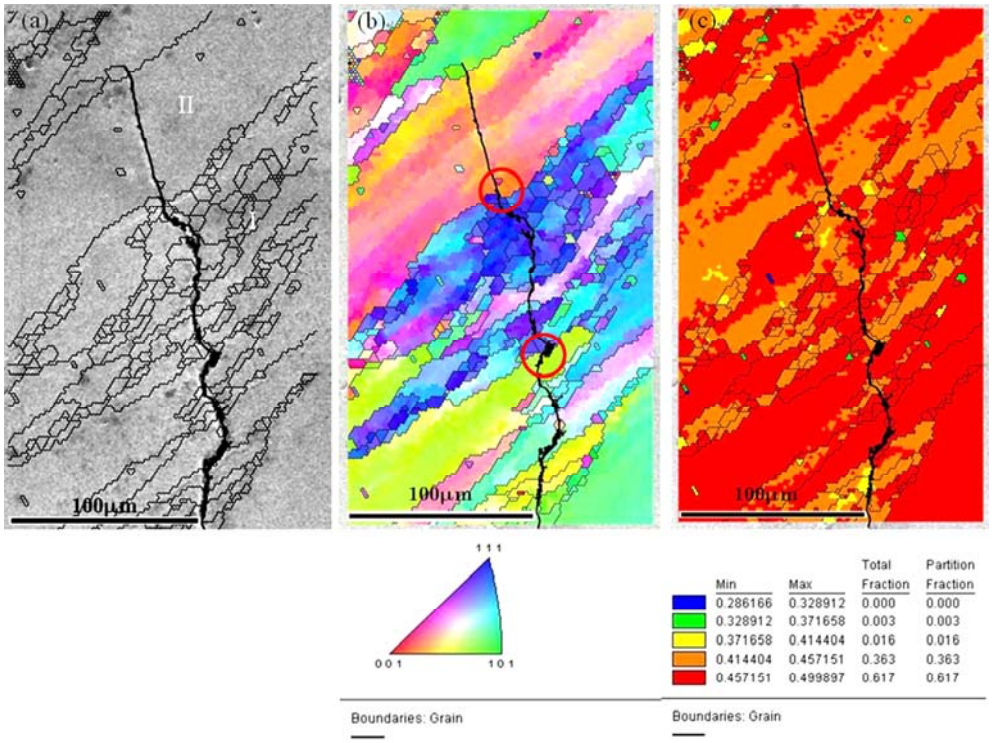

Fig. 5 EBSD image of fatigue crack early propagation paths of 2A97 alloy: (a) SEM image of fatigue crack and grain/sub-grain boundaries; (b) Grain orientation distribution; (c) Schmid factor distribution

preferably moves through the grains with a larger Schmid factor of the slip plane.

4 Discussion

The inclusions and coarsen secondary phases are the primary fatigue crack nucleation sites in 2A97 alloy, as shown in Fig. 3. Compared with the Al matrix, hard and brittle intermetallic compounds, such as $Al_7Cu_2(Fe,Mn)$ particles mentioned above, can be difficult to cut by dislocations, causing dislocation pile-up in the case of high stress or local stress concentration, and the micro-cracks are formed by the crushing of particles or the debonding at the interface between particles and matrix [19]. Besides, other locations such as the edges of the specimens, where there are regions for high stress concentration, or grain boundaries interacted strongly with slip bands or dislocations where strain localization and micro cracks are easily formed. The micro-cracks continue to expand in the matrix, and form the macroscopic cracks under the subsequent cyclic stress.

To reveal the relationship between the microstructures of grain boundaries, persistent slip bands and the fatigue crack early propagation behavior, TEM images of dislocation structures are shown in Figs. 6(a) and (b). The specimen is cyclic loading at 350 MPa for about 30000 cycles, when R=0.1 and K_t=1.0. The thin foils for TEM observations are shown near the crack tip. TEM images in bright field and dark field in Fig. 6 show several parallel gray or white stripes passing through grain (or sub-grain) boundaries, which are called slip bands. The closer grain contrast of grains I and II determines that there is a low-angle grain boundary between these two adjacent grains, and the strong grain contrasts of grains II and III, I and IV show that those are large-angle grain boundaries. It could be observed that the persistent slip bands pass easily through the I−II grain boundary without almost any significant deflection, while no apparent slip strips are shown in grains III and IV. This is corresponding to the previously mentioned mechanism proposed by SANGID et al [20]. The circular mark in Fig. 6(b) shows that the slip bands move straightly through the grain-boundary precipitate, and form a larger local stress concentration around grain boundary.

Figure 6(c) shows the relationship between grain boundary and persistent slip bands in relation to the fatigue crack early propagation behavior in 2A97 alloy. A large number of vacancies, dislocations and other defects exist around the grain boundary and its vicinity, subjecting to higher stress concentration. Meanwhile, the existence of the PFZs and the equilibrium phases arouses the weaker resistance to stress concentration and the micro-crack initiation relative to the matrix. Under the intense stress field at the tip of the micro-cracks, dislocations are easy to form pile-up at the grain

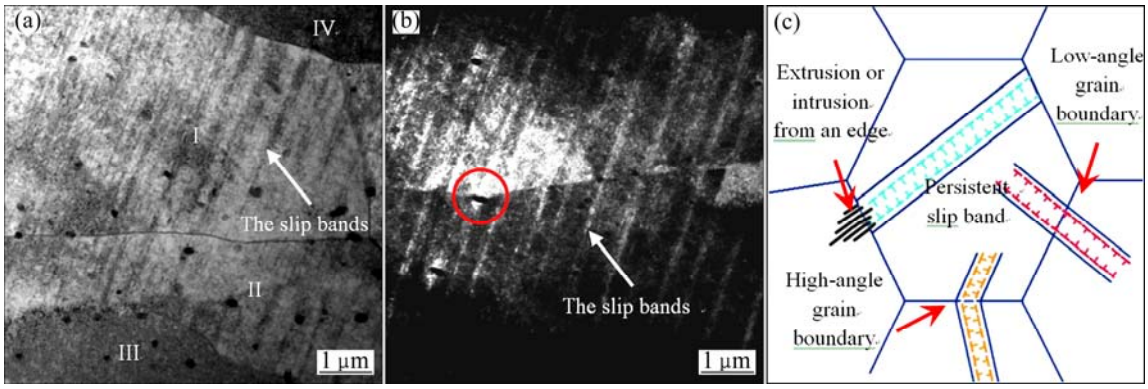

Fig. 6 TEM images of dislocation structures with σ_{max}=350 MPa, R=0.1 after 30000 cycles in bright field (a) and dark field (b), schematic of interaction between grain boundaries and PSBs (c)

boundaries, which makes strong stress concentration and produces a large amount of persistent slip bands. And the cycle slips can also leave the traces of extrusions and intrusions at the surface of the specimen, where the micro-cracks can initiate easily, especially at the specimen sharp edges.

The SEM images in Fig. 4 show that numerous traces of the PSBs form near the main crack, and some secondary cracks generate along these PSBs. The EBSD results in Fig. 5 indicate that fatigue cracks pass through high-angle grain boundaries with obvious large deflections, and move through low-angle sub-grain boundaries without almost no deflection or along the sub-grain boundaries. The Schmid factor distribution in Fig. 5(c) shows that the fatigue crack almost selects the most favorable path which has the maximum Schmid factor of slip system within one grain [7,21]. When the orientation difference of the favorable slip plane is small, which causes the slight impediment of grain boundary on the crack, the crack growth path is not prone to deflection. Otherwise, the crack is hard to move through grain boundary to the favorable slip plane of the adjacent grain, then the fatigue crack would deflect or terminate on the grain boundaries [20,22]. As the misorientation of two neighbouring grains is close to the orientations of the favorable slip plane within these two grains [8], low-angle grain boundary weakly hinders dislocations and the PSBs, so the PSBs can easily traverse straightly through adjacent grains. High-angle grain boundary has a strong blocking effect on the motion of dislocations, which impedes the PSBs traversing through grain boundary.

The slip bands are associated mainly with strong plastic deformation, while the specimen is predominantly under the elastic state. Under the cyclic stress, the strong interactions between the dislocations, precipitates and grain boundaries lead to intense stress concentrations, which may cause cyclic plastic deformations in local areas even when the loading stress is far below the yield stress, and these areas may become the places for crack initiation.

5 Conclusions

1) The coarsened secondary phases and inclusions are the primary fatigue crack nucleation sites in fatigue smooth specimens of 2A97 alloy. The cracks mainly initiate at the interior of large $Al_7Cu_2(Fe,Mn)$ particles, the aluminum oxides or defects and the vicinity of specimen sharp edge.

2) The fatigue crack early propagation behavior of 2A97 alloy is jointly influenced by precipitates, grain/sub-grain boundaries and their interactions with dislocations or persistent slip bands (PSBs). When the misorientation of two grains is close to the orientations of the favorable slip plane within these two grains, high-angle grain boundary plays as an obstacle role in the moving of the PSBs, thus leads to crack bifurcation and deflection. While low-angle grain boundary weakly hinders the PSBs passing through, so the crack growth path is not prone to deflection.

References

[1] MERATI A. A study of nucleation and fatigue behavior of an aerospace aluminum alloy 2024-T3 [J]. International Journal of Fatigue, 2005, 27(1): 33−44.

[2] LUKÁŠ P. Fatigue crack initiation mechanisms. Encyclopedia of materials: Science and technology [M]. 2nd ed. Oxford, Elsevier, 1992: 2882−2891.

[3] TANAKA K, MURA T. A theory of fatigue crack initiation at inclusions [J]. Metallurgical and Materials Transactions A, 1982, 13(1): 117−123.

[4] LAZ P, HILLBERRY B. Fatigue life prediction from inclusion initiated cracks [J]. International Journal of Fatigue, 1998, 20(4): 263−270.

[5] MORRIS W, JAMES M. Statistical aspects of fatigue crack nucleation from particles [J]. Metallurgical and Materials Transactions A, 1980, 11(5): 850−851.

[6] KUNG C, FINE M. Fatigue crack initiation and microcrack growth in 2024-T4 and 2124-T4 aluminum alloys [J]. Metallurgical and Materials Transactions A, 1979, 10(5): 603−610.
[7] ZHAI T, WILKINSON A, MARTIN J. A crystallographic mechanism for fatigue crack propagation through grain boundaries [J]. Acta Materialia, 2000, 48(20): 4917−4927.
[8] WEN W, ZHAI T. Three-dimensional effects of microstructures on short fatigue crack growth in an Al−Li 8090 alloy [J]. Philosophical Magazine, 2011, 91(27): 3557−3577.
[9] MORRIS W, JAMES M. Statistical aspects of fatigue crack nucleation from particles [J]. Metallurgical and Materials Transactions A, 1980, 11(5): 850−851.
[10] LIAO M. Dislocation theory based short crack model and its application for aircraft aluminum alloys [J]. Engineering Fracture Mechanics, 2010, 77(1): 22−36.
[11] RIOJA R J, LIU J. The evolution of Al−Li base products for aerospace and space applications [J]. Metallurgical and Materials Transactions A, 2012: 1−13.
[12] JIANG N, GAO X, ZHENG Z Q. Microstructure evolution of aluminum-lithium alloy 2195 undergoing commercial production [J]. Transactions of Nonferrous Metals Society of China, 2010, 20(5): 740−745.
[13] PRASAD N E, GOKHALE A, RAO P R. Mechanical behaviour of aluminium-lithium alloys [J]. Sadhana, 2003, 28(1): 209−246.
[14] ZHONG Shen, ZHENG Zi-qiao, LIAO Zhong-quan, CAI Biao. Effects of aging treatment on strength and fracture toughness of 2A97 aluminum-lithium alloy [J]. The Chinese Journal of Nonferrous Metals, 2011, 21(3): 546−553. (in Chinese)
[15] LI Hong-ying, WANG Xiao-feng, ZHAO Yan-kuo, ZENG Cui-ting, ZHANG Jian-fei. Effect of solution temperature on microstructure and properties of 2A97 alloy [J]. Transactions of Materials and Heat Treatment, 2010, 31(4): 114−119. (in Chinese)
[16] YUAN Z S, WU X L , LU Z , XIE Y H, DAI S L , LIU C S. The aging behavior of aluminum-lithium alloy 2A97 [J]. Rare Metal Materials and Engineering, 2008, 37(11): 1898−1902. (in Chinese)
[17] TERRONES L A H, MONTEIRO S N. Composite precipitates in a commercial Al−Li−Cu−Mg−Zr alloy [J]. Materials Characterization, 2007, 58(2): 156−161.
[18] FRAGOMENI J, WHEELER R, JATA K. Effect of single and duplex aging on precipitation response, microstructure, and fatigue crack behavior in Al−Li−Cu alloy AF/C-458 [J]. Journal of Materials Engineering and Performance, 2005, 14(1): 18−27.
[19] BOWLES C, SCHIJVE J. The role of inclusions in fatigue crack initiation in an aluminum alloy [J]. International Journal of Fracture, 1973, 9(2): 171−179.
[20] SANGID M D, MAIER H J, SEHITOGLU H. The role of grain boundaries on fatigue crack initiation-An energy approach [J]. International Journal of Plasticity, 2011, 27(5): 801−821.
[21] LI J, ZHAI T, GARRATT M, BRAY G. Four-point-bend fatigue of AA 2026 aluminum alloys [J]. Metallurgical and Materials Transactions A, 2005, 36(9): 2529−2539.
[22] SANGID M D, EZAZ T, SEHITOGLU H, ROBERTSON I M. Energy of slip transmission and nucleation at grain boundaries [J]. Acta Materialia, 2011, 59(1): 283−296.

2A97 铝锂合金的疲劳裂纹萌生及早期扩展行为

钟 警[1]，钟 申[1]，郑子樵[1,2]，张海锋[1]，罗先甫[1]

1. 中南大学 材料科学与工程学院，长沙 410083；
2. 中南大学 有色金属材料科学与工程教育部重点实验室，长沙 410083

摘 要：研究 2A97 铝锂合金的疲劳裂纹萌生及早期扩展行为。在室温条件下，采用光滑试样进行疲劳测试，其中最大应力为恒定值，应力比 R 为 0.1，频率 f 为 40 Hz。利用金相显微镜、透射电镜、扫描电镜及电子背散射衍射等手段对合金的微观组织进行分析，研究合金的疲劳裂纹萌生及早期扩展行为与其微观组织的关系。结果表明：2A97 合金的疲劳裂纹主要萌生于试样表面的杂质相和粗大第二相处；其疲劳裂纹的早期扩展行为主要受晶粒结构与位错或滑移带共同作用的影响。当相邻晶粒的错配度接近于其晶内的最优滑移面的位向差时，大角度晶界强烈阻碍滑移带的运动，从而导致裂纹分叉和偏折。

关键词：2A97 铝锂合金；疲劳裂纹萌生；早期扩展

(Edited by Chao WANG)